Monthly Notices of the ROYAL ASTRONOMICAL SOCIETY

MNRAS **524,** 2368–2378 (2023) https://doi.org/10.1093/mnras/stad1970
Advance Access publication 2023 June 30

Collision-induced excitation of ammonia in warm interstellar and circumstellar environments

Sándor Demes [1]★ François Lique,[1]★ Jérôme Loreau [2] and Alexandre Faure [3]

[1] *Univ Rennes, CNRS, IPR (Institut de Physique de Rennes) - UMR 6251, F-35000 Rennes, France*
[2] *KU Leuven, Department of Chemistry, B-3001 Leuven, Belgium*
[3] *Université Grenoble Alpes, CNRS, IPAG, F-38000 Grenoble, France*

Accepted 2023 June 28. Received 2023 June 28; in original form 2023 June 20

ABSTRACT

Ammonia (NH_3) is the first polyatomic molecule detected in the interstellar medium. Both its spectroscopic and collisional properties have been extensively studied earlier, and NH_3 has often been used in laboratory astrophysics studies to compare high-level scattering calculations with state-of-the-art experiments. Nevertheless, some of its important collisional properties remain unresolved. In this paper, we report state-to-state and thermally averaged collisional data for the rotational excitation of NH_3 by H_2 calculated with the close-coupling quantum theory. Both nuclear spin symmetries (*ortho*/*para*) of the colliders are studied. Similar research has been carried out previously, providing rate coefficients up to a temperature of 200 K for rotational states with internal energy up to $\sim$420 cm^{-1}. Here, we have computed cross sections for collision energies up to 4700 cm^{-1} and rate coefficients up to 500 K. Most of the rotation-inversion levels of ammonia have been considered below the first vibrational excitation threshold, leading to a total of 33 *ortho*- and 62 *para*-NH_3 states. We have compared our results with the most accurate data for He and H atoms available in the literature. The propensity rules have also been analysed in the case of high rotational levels of NH_3. The rate coefficients obtained by averaging over the thermal H_2 relative populations exhibit significantly larger magnitudes than the state-to-state collisional data in the case of NH_3 transitions with large internal energy difference, when the rotational energy transfer between the colliders is strong.

Key words: astrochemistry – molecular data – molecular processes – methods: laboratory: molecular – ISM: molecules.

1 INTRODUCTION

The first polyatomic molecule detected in the interstellar medium (ISM) was ammonia (NH_3) (Cheung et al. 1968). Since the beginning of the era of radio astronomy, ammonia has gained great astronomical importance due to its specific and very favourable spectroscopic properties. Due to the features of its inversion-rotation transitions, which allow the detection of highly excited NH_3 lines, ammonia has been widely used to probe the physical conditions in a variety of interstellar environments (see the early review by Ho & Townes (1983) on the interstellar importance of ammonia). Consequently, NH_3 as well as its isotopologues are actively targeted in observational molecular astrophysics today, as indicated by numerous research papers in the past few years (Mills & Morris 2013; Mills et al. 2018; Wong et al. 2018; Gao et al. 2019; Sipilä et al. 2019; Zhou et al. 2020; Bőgner et al. 2022; De Simone et al. 2022; Feng et al. 2022; Galloway-Sprietsma et al. 2022; Candelaria et al. 2016). Some of these observations (see e.g. De Simone et al. 2022; Candelaria et al. 2016) report highly excited rotational lines of ammonia in warm interstellar environments. However, to adequately interpret such observations in intersteallar clouds, accurate collisional data are required, as the population of rotational levels is dominantly determined by the competition between radiative and collisional processes (Bouhafs et al. 2017). Rotationally inelastic collisions of NH_3 with the most abundant interstellar atoms and molecules (H_2, H, He) are the most important processes from the point of view of astrophysical environments, including interstellar clouds, photodissociation regions (PDRs), pre-stellar cores as well as external galaxies. Even though a large number of sophisticated measurements have been carried out previously to study low-energy collisions of NH_3 with H_2 and other important colliders (see, for example, Daly & Oka 1970; Schleipen, ter Meulen & Offer 1993; Willey et al. 2002), the experiments usually do not provide direct state-to-state rate coefficients, which are the most important collisional quantities from an astrophysical point of view.

Up to this point, numerous theoretical investigations have been devoted to the study NH_3–H_2 collisions, including the early study by Danby et al. (1988), which did not consider the rotational structure of hydrogen, assuming a collision with *p*-H_2 ($j_{H_2} = 0$). The NH_3–H_2 theoretical studies were later significantly improved by Maret et al. (2009) and then by Ma et al. (2015). It is also worth mentioning the accurate scattering calculations for deuterated isotopologues such as NHD_2, NH_2D, ND_3 performed by Daniel et al. (2014, 2016). Rotationally inelastic differential cross sections have also been measured and calculated for ND_3 in collision with H_2 (Tkáč et al. 2015) and D_2 (Gao et al. 2019) at some very limited collision energies. The satisfactory agreement between theory and experiment reported in these works could be referred to as a good probe of the

★ E-mail: sandor.demes@univ-rennes1.fr (SD); francois.lique@univ-rennes.fr (FL)

accuracy of the methods commonly used in potential energy surface (PES) and scattering calculations. Although ammonia appears to be an extremely well studied system from this point of view, there are still several limitations on the existing collision data. The most complete set of data for NH_3–H_2 collision is provided by Bouhafs et al. (2017), where the authors studied all rotational transitions between levels with internal energies below 417 cm^{-1} and provided rate coefficients up to kinetic temperature of 200 K.

Apart from collisions with H_2, a large number of experimental and theoretical studies have been devoted to the study of inelastic collisions of ammonia with other projectiles, dominantly by atomic species like H, He, Ar, Xe, Rb, *etc.* From an astrophysical point of view, the most important of these are the NH_3–He and NH_3–H collisions, the former being often used as a template for H_2. The NH_3–He collision has been extensively studied since the first NH_3 observations (see the measurement by Oka (1968) and the calculation by Green (1980)). For astrophysical applications, the most complete set of rate coefficients for collisions with helium is given by Machin & Roueff (2005), where the authors calculated accurate cross sections up to 1500 cm^{-1} and rate coefficients up to 300 K. Later Yang & Stancil (2008) reproduced the rate coefficients of Machin & Roueff (2005), and significantly extended their range towards mK temperatures. While the authors of this work have also extended the collision energy range (from 10^{-5} up to 10^4 cm^{-1}), unfortunately their work covers low-lying ammonia levels only (with internal energies below $\sim$200 cm^{-1}), which severely limits their astrophysical use.

It should be stressed again that without accurate and broadband collisional rate coefficients, the abundance of NH $_3$ molecules in warm interstellar clouds could only be approximated, under the assumption of local thermodynamic equilibrium (LTE) conditions, which is usually not a good approximation in such media (Roueff & Lique 2013). Therefore, in the present work, we provide a complete set of collisional cross sections and thermal rate coefficients for the rotational excitation of NH_3 by H_2, calculated on the basis of an accurate and well-tested 5-dimensional interaction potential (Maret et al. 2009). The new collisional data have several crucial improvements over the results of Bouhafs et al. (2017): first, the present calculations include all rotational levels with internal energies up to $\sim$800 cm^{-1}, and second, the rate coefficients are calculated up to higher temperatures (500 K). The paper is structured as follows: In Section 2, the details of the interaction potential (Subsection 2.1) as well as the scattering calculations (Subsection 2.2) are presented. The state-to-state collisional data are analysed and discussed in Section 3, with Subsection 3.1 devoted to the cross sections, Subsection 3.2 to the thermal rate coefficients, and Subsection 3.3 to the collisional propensity rules. Our concluding remarks are given in Section 4.

2 METHODS

2.1 Potential energy surface

For the NH_3–H_2 interaction potential, we have used the five-dimensional PES proposed by Maret et al. (2009), in which all intramolecular coordinates are kept fixed (rigid rotor approximation). As it was discussed earlier by Maret et al. (2009) and later by Bouhafs et al. (2017), due to the good agreement between the theory based on this PES and the laboratory measurements, such an approximation is considered appropriate for collision energies below the first vibrational excitation threshold of ammonia ($\nu_2 = 1$), *i.e.* at $E_c < 932.4$ cm^{-1} (Rajamäki, Miani & Halonen 2003), provided that the collision time-scales are faster than the inversion vibrational motion of ammonia. This allows one to compute reliable collisional rate coefficients at least up to 500 K kinetic temperatures.

Since the PES of Maret et al. (2009) has already been described in detail (see also Bouhafs et al. 2017), we only briefly summarize its main points:

(i) For the geometries of the monomers, the ground-state averaged bond lengths r and bond angles α were used ($r_{N-H} = 1.9512$ a_0, $\alpha_{H-N-H} = 107.38^\circ$ for NH_3 and $r_{H-H} = 1.4488$ a_0 for H_2), as it was shown to be the most appropriate in the full-dimensional study of H_2O–H_2 collision by Faure et al. (2005).

(ii) The analytical PES was fitted on 29 000 *ab initio* CBS-extrapolated reference points with a 167-term angular expansion (including anisotropies up to $l_1 = 10$ and $l_2 = 4$) using a Monte Carlo error estimator (Rist & Faure 2012). The *ab initio* points were calculated using standard coupled-cluster theory with singles and doubles and perturbative corrections for triple excitations [CCSD(T)], with a simple complete basis set (CBS) extrapolation procedure.

(iii) The accuracy of the final fit is <1 cm^{-1} both in the long-range part and in the well region of the PES ($R \gtrsim 5$ a_0, where R is the intermolecular distance between the centres of mass of the colliders).

(iv) The global minimum is about -267 cm^{-1} located at $R = 6.1$ a_0.

We have used the following units throughout this paper (unless otherwise noted): atomic units (a_0) for distances (1 $a_0 \approx 5.29177 \times 10^{-9}$ cm), wave numbers (cm^{-1}) for energies (1 $cm^{-1} \approx 1.4388$ K).

2.2 Scattering calculations

In this work, we have computed state-to-state rotational (de)excitation cross sections and thermal rate coefficients for the collision of *ortho*(o)- and *para*(p)-NH_3 with both *ortho*- and *para*-H_2. Previously, similar calculations were performed by Bouhafs et al. (2017) for collision energies of 0.1–1600 cm^{-1}, including rotational states with internal energies up to 417 cm^{-1}. Our current work is an extension of this latter with several substantial improvements. Most importantly, we have significantly increased the number of states, involving all rotation-inversion levels up to 800 cm^{-1} (*i.e.* somewhat below the first vibrational excitation threshold of NH_3 at $\nu_2 \simeq 932.4$ cm^{-1}), which can be treated effectively within the limits of the rigid-rotor approximation. Consequently, we have also greatly increased the collision energy range, allowing very accurate thermal rate coefficients to be derived up to 500 K, and with some limitations even up to 800 K. This is a significant improvement compared to the work of Bouhafs et al. (2017), where the largest kinetic temperature presented is 200 K.

The general methodology we used in the current work is very similar to that previously applied by Bouhafs et al. (2017). In order to avoid discrepancies between different theories, we did not use any approximate methods (*e.g.* coupled states), and we calculated the cross sections by the most accurate close-coupling (CC) quantum approach in the whole energy range, using the recent version 5 of the `HIBRIDON` scattering code (Alexander et al. 2023). In the case of collisions with p-H_2 projectiles, they were computed up to a total energy of 4500 cm^{-1}, while for o-H_2 energies up to 4700 cm^{-1} were considered. As described in detail by the authors of previous NH_3 studies (Danby et al. 1988; Rist, Alexander & Valiron 1993; Maret et al. 2009; Bouhafs et al. 2017), the rotation-inversion levels of a symmetric top molecule can be denoted by j_k^ϵ, where j is the total angular momentum quantum number, and k is its projection on the C_3 principal rotational axis, while ϵ is the symmetry index (Rist et al.

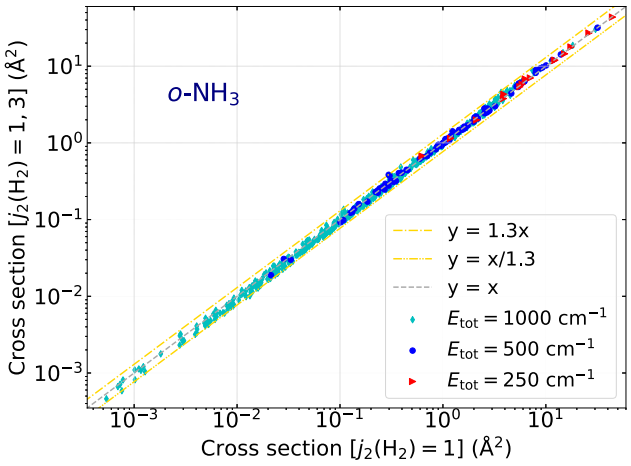

Figure 1. Ratio of the state-to-state cross sections for the o-NH_3–o-H_2 collision as computed with ($j_2 = 1$) versus ($j_2 = 1, 3$) rotational basis sets. All possible de-excitation transitions are compared at 250, 500, and 1000 cm^{-1} total energies (E_{tot}).

1993). In order to be consistent with the spectroscopy literature, in the present work we use the following $j_k^{\pm}$ notation, involving the inversion symmetry (defined as $+/- = -\epsilon(-1)^j$), contrary to Bouhafs et al. (2017), who used the ϵ symmetry index. *Ortho*-NH_3 requires that $k = 3n$ (n are integer numbers), while all other k quantum numbers refer to *para*-NH_3, defining about twice as many rotational levels in favour of the latter below a certain internal energy limit. It is worth mentioning that the electric dipole transition rules prevent radiative transitions to occur between different k-ladders ($\Delta j = 0,\pm1$; $\Delta k = 0$; $\epsilon = \pm$), so the lowest inversion doublets in each $k > 0$ ladder are metastable and can only be relaxed through collisions (Maret et al. 2009).

We have calculated the collisional data for transitions between all rotational states below ~800 cm^{-1}, including levels up to 10_9^- for o-NH_3 and 9_5^- for p-NH_3, thus all states with $j \leq 8$ (and also some of those with $j = 9$ and 10) are studied. For a detailed list of the rotational levels considered in this work, see Tables A1 and A2 in Appendix A. In the case of the H_2 projectile, the three lowest rotational states are considered in the scattering calculations, including $j_2 = 0$, 2 for p-H_2 and only $j_2 = 1$ for o-H_2 (j_2 refers to the rotational state of H_2 throughout the paper). The collisional data calculated with a larger $j_2 = 1$, 3 basis for o-H_2 imply rather small differences as compared to the results obtained with a smaller $j_2 = 1$ basis (see Fig. 1). The systematic comparison of all state-to-state cross sections at some particular total energies (since large-scale scattering calculations with $j_2 = 1$, 3 are unfeasible) shows that the larger o-H_2-basis has no significant impact on the results, the average errors between the two data sets presented in Fig. 1 vary only between 3.7 per cent (at 250 cm^{-1}) and 7.6 per cent (at 1000 cm^{-1}). The contribution from a larger H_2 rotational basis is usually <10 per cent, and higher rotational terms ($j_2 > 3$) would have even less remarkable effects on the collisional data. It is worth noting that due to the wide range of collision energies, we have computed many transitions with the $j_2 = 2$ excited state of H_2 as the collider, which has not been done in any of the previous works. Since all four nuclear spin combinations are treated separately (the selection rules prevent *ortho*-to-*para* transitions), the calculations involving the p-NH_3 species are computationally more expensive, which is also the case with p-H_2, due to the larger rotational basis.

As is typical for full quantum CC calculations, both the rotational basis (j_{max}) and the maximum total angular momentum (J_{tot}) values were constrained depending on the collision energy. Their particular values were determined from the results of systematic convergence test calculations, using the following thresholds: in the case of the rotational basis size, a maximum mean deviation criteria of 1 per cent was set for total energies up to 2000 cm^{-1}, which was then gradually increased up to 5 per cent at the highest energies (>4000 cm^{-1}), leading to j_{max} up to 17. The largest total angular momentum parameters were set by stricter convergence-threshold criteria: a maximum of 0.01 per cent mean deviation was allowed up to 2000 cm^{-1}, which was increased up to 0.1 per cent at higher energies. We used the Airy propagator at long-range radial distances and the log-derivative propagator in the short range. The best parameters for the propagator model (*i.e.* the initial and final distance of propagation and the switching point between the two propagators) were also chosen by convergence tests, so that the mean deviation in the cross sections never exceeds 0.01 per cent due to these parameters. Finally, we also found an upper boundary for the significant rotational levels, which is about 1550 cm^{-1}. Excluding all levels above this threshold does not change the cross sections by more than 0.01 per cent on average, while such a limitation on the levels can save considerable computational time. Bouhafs et al. (2017) showed that the NH_3–H_2 cross sections are characterized by strong and dense resonances caused by the potential well (*i.e.* at collision energies up to ~267 cm^{-1}). Consequently, a rather small energy step size should be used in the scattering calculations. We applied $E_{step} = 1.0\,cm^{-1}$ up to 1200 cm^{-1} total energy, which was then gradually increased until 100 cm^{-1} at the highest energies.

The rate coefficients were calculated by integration over a Maxwell–Boltzmann distribution of relative velocities as follows:

$$k_{i\to f}(T) = \left(\frac{8}{\pi\mu k_B^3 T^3}\right)^{\frac{1}{2}} \int_0^\infty \sigma_{i\to f} E_c e^{-\frac{E_c}{k_B T}}\, dE_c. \quad (1)$$

Here, E_c is the collision or kinetic energy, $\sigma_{i\to f}$ is the cross section for a transition from a particular initial state (i) to a given final state (f), μ is the reduced mass of the 'projectile + target'molecular system, and k_B is the Boltzmann constant. It is necessary to mention that the computed cross sections would allow to obtain rate coefficients up to ~800 K, however, at such temperatures, the rotational levels above the $\nu_2 = 1$ vibrational threshold can be significantly populated (effectively up to about ~1500 cm^{-1}). These high-lying states are not straightforward to implement in our CC-formalism, first, due to the lack of vibrational dependence in the PES, and second, since the total number of levels would be extremely large, making the calculations not feasible (with our calculations we reached about 11 000 as a maximum number of coupled channels, which is pushing the currently accepted upper limit of the CC-formalism). Also, at these temperatures, we should consider more H_2-levels ($j_2 = 3$–5), since they can also be efficiently populated. We should keep in mind then that our collisional data would not be complete at 800 K due to the lack of significantly populated states, both in terms of NH_3 and H_2 levels, which may lead to unknown uncertainties in radiative transfer models. Our calculations show that the inclusion of higher levels does not change the cross sections below $\nu_2 = 1$, so we can confirm that the collisional data reported in this work, which include all ammonia levels below ~800 cm^{-1}, are consistent and robust. The rotational levels of H_2($j_2 = 0$–2) considered in this work allowed one to compute accurate collisional data for all NH_3-transitions involving these states up to 500 K kinetic temperature. According to our rough estimations, a total of about 1.5 million CPU-hours have been spent to perform the scattering calculations reported in this work.

In addition to the state-to-state collisional data, we also report thermally averaged rate coefficients with respect to the H_2 projectile in order to efficiently model excitation of ammonia in warm environments. For any transitions of the target molecule, the rate coefficients averaged over a thermal distribution of the H_2 projectile can be obtained as follows:

$$\overline{k}_{j\to j'}(T) = \sum_{j_2} n_{j_2}(T) \sum_{j_2'} k_{jj_2\to j'j_2'}(T), \tag{2}$$

where $n_{j_2}(T)$ is the relative population of the projectile:

$$n_{j_2}(T) = \frac{(2j_2+1)\exp\left(-\frac{E_{j_2}}{k_B T}\right)}{\sum_{j_2'}(2j_2'+1)\exp\left(-\frac{E_{j_2'}}{k_B T}\right)}. \tag{3}$$

In equations (2–3), j and j' denote the initial and final rotational levels of ammonia (defined by the j, k, ϵ quantum numbers), j_2 and j_2' refer to the initial and final rotational states of H_2, respectively, while E_{j_2} and $E_{j_2'}$ are the corresponding internal energy of the projectile. The sum $(2j_2 + 1)$ defines the degeneracy of the particular H_2 levels for a particular nuclear symmetry. We computed thermalized rate coefficients for all NH_3 transitions induced by p-H_2 in $j_2 = 0$ and 2. Higher levels ($j_2 > 2$) are not significantly populated at temperatures below 500 K. In the case of o-H_2, we cannot provide thermalized rate coefficients due to the lack of data with the $j_2 = 3$ collider, but since the results obtained with o-$H_2(j_2 = 1)$ are in a fairly good agreement with the thermally averaged p-H_2 data, one can assume that thermalized rate coefficients are those with $j_2 = 1$. Somewhat larger deviations are found for a few transitions only, which are related to near-resonant effects. It is worth to mention that, since the rate coefficients are computed below 500 K only, near-resonance effects due to $j_2 = 1 \leftrightarrow 3$ transitions (which involves an energy transfer of $\sim$587 cm^{-1}) can be neglected.

3 RESULTS AND DISCUSSION

3.1 Cross sections for rotational excitation

In Figs 2 and 3, the variation of the state-to-state rotational de-excitation cross sections is presented for some selected transitions of NH_3 as a function of the collision energy. Our current results for collisions with $o-H_2(j_2 = 1)$ and p-H_2 (both $j_2 = 0$ and 2) are compared with the most accurate data for collisions with atomic hydrogen (Bouhafs et al. 2017) and helium (Yang & Stancil 2008). We do not aim to make a comparison with the most recent NH_3–H_2 theoretical data from Ma et al. (2015); Bouhafs et al. (2017), since these authors used a very similar methodology and PES, so their results are in a perfect agreement with ours for the common transitions. Those transitions of NH_3 are also presented in which p-H_2 is changing its rotational state, (these are the so-called H_2-inelastic processes). We considered two of these, which are relevant at temperatures <500 K: the $j_2 = 0 \to 2$ excitation and the $j_2 = 2 \to 0$ de-excitation process. For sake of clarity, in the remainder of the text, we will indicate both the initial and final levels of H_2 even for elastic transitions (*e.g.* $j_2 = 0 \to 0$ for the collision with ground state p-H_2, *etc*).

Fig. 2.a shows the cross sections for the transition from the first excited state of o-NH_3 (1_0^+) to its ground state (0_0^-). As can be seen, significant differences are found depending on the type of the projectile (o/p-H_2, H or He). For example, collisions with helium are characterized by much smaller cross sections compared to the data for H_2 or even atomic H projectiles. With respect to H_2, the

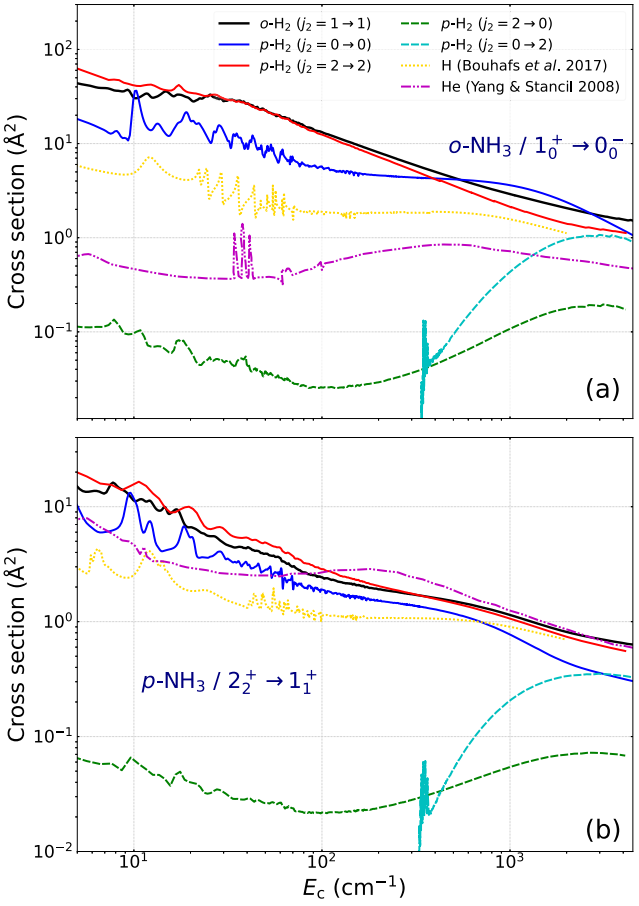

Figure 2. The variation of rotational de-excitation cross sections for the $1_0^+ \to 0_0^-$ transition of o-NH_3 (panel a) and $2_2^+ \to 1_1^+$ transition of p-NH_3 (panel b). The collisions with o-$H_2(j_2 = 1 \to 1)$ and p-H_2 (all states involving $j_2 = 0$ and 2) are compared with the corresponding results of Bouhafs et al. (2017) for collision with H and those of Yang & Stancil (2008) with He.

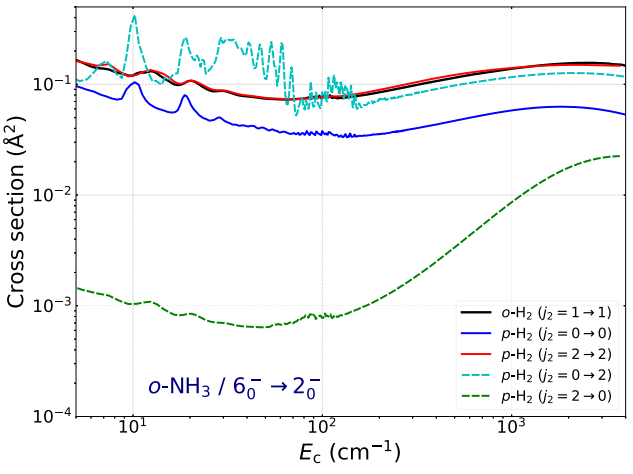

Figure 3. The variation of the near-resonant $6_0^- \to 2_0^-$ rotational transition of o-NH_3 in collision with p-H_2 (involving all state-changing and state-conserving processes with $j_2 = 0$, 2) as well as with o-$H_2(j_2 = 1 \to 1)$.

differences can be more than an order of magnitude, especially in the low-energy regime (below ∼100 cm^{-1}). As the collision energy increases, the cross sections become somewhat closer to each other, but the differences are still very significant (at least a factor of 8 around ∼500 cm^{-1}). As also observed previously for H_2O (Daniel, Dubernet & Grosjean 2011) and NH_2D (Daniel et al. 2016), the cross sections for collisions with ground state o-$H_2(j_2 = 1 \rightarrow 1)$ and with excited p-$H_2(j_2 = 2 \rightarrow 2)$ are quite close in general, although at low collision energies $j_2 = 2$ is somewhat larger, while the opposite is true at high energies. The differences increase slowly with increasing E_c and reach a maximum of about a factor of 1.5. However, the cross sections involving ground state p-$H_2(j_2 = 0 \rightarrow 0)$ are significantly different: they are quasi-constant at $E_c \sim$ 100–1000 cm^{-1}, are usually much lower in magnitude than the other H_2-elastic data, and are characterized by a superimposed, dense resonant structure. A similar behaviour has been found by Lanza et al. (2014) when comparing the cross sections calculated for the HCl molecule in collision with ground-state o/p-H_2 and excited p-$H_2(j = 2)$ projectiles. These differences are related to the properties of the PES and its expansion coefficients. While the $NH_3 - p$-$H_2(j_2 = 0 \rightarrow 0)$ scattering matrices and cross sections depend only on the $l_2 = 0$ terms of the interaction potential (l_2 is the tensor rank which defines the angular dependence on the H_2 orientation, see Rist et al. (1993) for details), higher H_2-levels ($j_2 > 0$) are also affected by the $l_2 = 2$ ($j_2 = 1$) and $l_2 = 2, 4$ ($j_2 = 2$) expansion terms (note that l_2 must be even for homonuclear diatoms). In particular, the quadrupole behaviour of H_2 (represented by the $l_2 = 2$ term) plays an important role at long-range. Since the magnitude of the $l_2 = 2$ terms is comparable to that of the $l_2 = 0$ terms, larger cross sections are observed for the $NH_3 - o$-$H_2(j_2 = 1)$ scattering process. However, the terms $l_2 \geq 4$ are negligible compared to $l_2 = 0$, 2. It is worth noting that the o-H_2 and p-$H_2(j_2 = 2)$ cross sections also involve multiple resonances, but they are very close together, leading to a strong overlapping and broadening, and thus these resonance peaks cannot be clearly identified. If we examine the $1_0^+ \rightarrow 0_0^-$ NH_3 transition accompanied with the $j_2 = 0 \rightarrow 2$ H_2-inelastic process, we can clearly see the threshold above ∼337 cm^{-1}, where this channel opens, and right above this a strong, dense resonance behaviour. The corresponding cross sections then increase rapidly, approaching the magnitude of the H_2-elastic cross sections at higher collision energies. Due to this, such process can have a significant impact on the high-temperature thermalized rate coefficients. The transition accompanied with H_2 de-excitation ($j_2 = 2 \rightarrow 0$) is somewhat different. It does not have a threshold, but at low collision energies it is by about two orders of magnitude lower than all other processes. The cross section of this process does not vary strongly with the energy, however it exhibits a wide, shallow minimum centred around 100 cm^{-1}. The impact of this process on the rate coefficients is rather negligible even at higher kinetic temperatures.

In the case of the $2_2^+ \rightarrow 1_1^+$ transition of p-NH_3 (Fig. 2.b), the overall trends are similar. A remarkable difference is that above ∼100 cm^{-1} collision energies, the cross sections for helium are slightly larger than all our H_2 data. This can be related to a broad maximum in the He cross sections, which is probably associated to the formation of shape (orbiting) resonances due to the opening of some initially closed channels above the van der Waals region of the NH_3–He PES (see Yang & Stancil (2008) for details). The cross sections for collisions with atomic hydrogen are usually lower than all other data, except for collision energies $\gtrsim$800 cm^{-1}, where they are comparable to or even exceed the p-H_2 ($j_2 = 0 \rightarrow 0$) cross sections. It is also worth mentioning that these cross sections generally possess very similar resonance structures qualitatively as compared to the corresponding data with ground-state p-H_2 projectile. This is related to the similar characteristics and shape of their interaction potentials, considering only the $l_2 = 0$ terms in the NH_3–H_2 PES.

Fig. 3 shows the cross sections for a near-resonant transition. In the case of a near-resonant transition, the internal energy change within the target molecule is accompanied with a very close internal energy change within the projectile. Such effects were studied in detail earlier for collision of HCl with H_2 by Lanza et al. (2014). The $6_0^- \rightarrow 2_0^-$ NH_3 transition with an energy gap of ∼356.5 cm^{-1} is quasi-resonant with the $j_2 = 0 \rightarrow 2$ transition in p-H_2 (∼356.3 cm^{-1}). The energy released by de-excitation of NH_3 can be almost entirely transferred to H_2, which is efficiently excited from $j_2 = 0$ to 2. On the other hand, the H_2 de-excitation ($j_2 = 2 \rightarrow 0$ process) releases such a portion of energy, which can be captured by NH_3, initiating a very efficient excitation in it ($2_0^- \rightarrow 6_0^-$). We can see in Fig. 3 a very pronounced near-resonant rotational energy transfer. The $j_2 = 0 \rightarrow 2$ cross section is very large, comparable with the H_2-elastic cross sections for all collision energies. Below ∼150 cm^{-1}, when the rotational energy transfer is the most efficient, its magnitude exceeds that of all H_2 state-conserving processes. In this energy interval, it shows a very pronounced resonance structure. Due to near-resonant effects the corresponding NH_3 de-excitation transition exhibit significantly larger thermalized rate coefficients as compared to any of the pure H_2-elastic processes.

Based on the comparative analysis of the cross sections, one can draw a conclusion that generally they do not correlate well with respect to the type of collider. We found no clear scaling rules between the collisional data calculated with $H_2(j_2 = 0, 1, 2)$ and those with He or H. These dissimilarities and random trends between the cross sections are expected to be present in the rate coefficients as well. The only relatively good agreement (within a factor of ∼1.5) is observed between the o-$H_2(j_2 = 1)$ and excited p-H_2 ($j_2 = 2$) cross sections. As a consequence, neither He nor H atomic colliders, nor the structureless ground state p-H_2 can be used as a template for collisions with molecular hydrogen at temperatures where its excited states ($j_2 \geq 1$) are effectively populated, *i.e.* at $T_{kin} > 100$ K. This has also been reported previously by several authors, see for example the review by Roueff & Lique (2013). Also, the cross sections can be strongly affected by near-resonant rotational energy transfer in the case of transitions from higher initial levels of NH_3, which is necessary to take into account when computing the rate coefficients.

3.2 Rate coefficients

Once the state-to-state cross sections were calculated, the corresponding thermal rate coefficients $k(T)$ were derived for all four nuclear spin combinations of the NH_3–H_2 collision. In the case of p-H_2 collider, in addition to the state-to-state collisional data, we also report the thermally averaged rate coefficients over the $j_2 = 0, 2$ levels.

In Fig. 4, we examine the temperature dependence of the rate coefficients for a fundamental ($1_0^+ \rightarrow 0_0^-$) and a near-resonant ($6_0^- \rightarrow 2_0^-$) rotational transition of o-NH_3. Since the $j_2 = 1 \rightarrow 1$ o-H_2 rate coefficients are very close to the $j_2 = 2 \rightarrow 2$ excited p-H_2 data, we decided not to show them separately, but we also show the thermally averaged rate coefficients computed for p-H_2. The general trends are similar to what was observed in the case of the cross sections. As one can see in Fig. 4a, when the transition energy is low, the H_2-inelastic transitions are very weak and the thermalized rate coefficients are only governed by the H_2-elastic processes. Due to the variation of

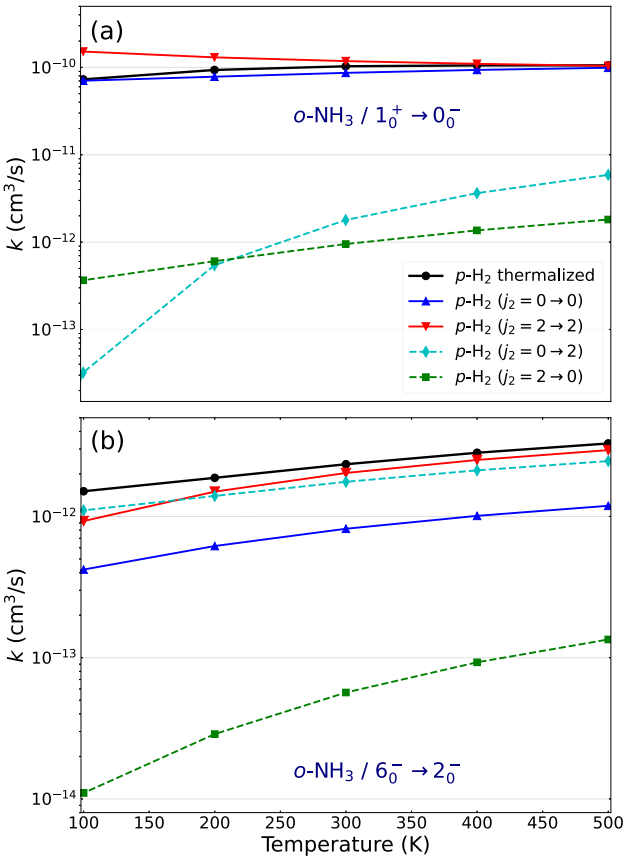

Figure 4. Thermal rate coefficients as a function of kinetic temperature for a fundamental low-energy ($1_0^+ \rightarrow 0_0^-$, panel a) and a near-resonant ($6_0^- \rightarrow 2_0^-$, panel b) o-NH_3 de-excitation transition calculated in collision with p-H_2 state-changing and state-conserving processes.

the H_2 population, the thermal average is always found to be between the $j_2 = 0 \rightarrow 0$ and $j_2 = 2 \rightarrow 2$ data: at low temperatures closer to the ground state, at 300 K along their average, while at 500 K close to the excited p-H_2 data. This trend is not valid, however, when the rotational energy transfer between the colliders is more efficient (the internal energy change $\Delta E_{\rm int}$ is large), especially in the case of near-resonant energy transfer. As one can see in Fig. 4b, in the case of the $6_0^- \rightarrow 2_0^-$ process with $\Delta E_{\rm int} \simeq 356.5\,{\rm cm}^{-1}$, the $j_2 = 0 \rightarrow 2$ H_2-excitation process is very strong and significantly contributes to the thermal average. Due to this, the thermalized rate coefficients can be even higher than the $j_2 = 2 \rightarrow 2$ (and thus $j_2 = 1 \rightarrow 1$) H_2-elastic data. Since the $j_2 = 0 \rightarrow 2$ process is involved in the thermal average with a weight given by the relative population of its $j_2 = 0$ state, this effect is more pronounced at 100 K. The $j_2 = 2 \rightarrow 0$ H_2-inelastic rate coefficients are very weak, as expected.

The relative ratios of the rate coefficients are also analysed to compare the magnitude and the variation of $k(T)$ with respect to the state of the H_2-projectile. Fig. 5 shows a comparison of the rate coefficients for all rotational transitions considered for o-NH_3 (with $E_{\rm int} \lesssim 800\,{\rm cm}^{-1}$) in collision with o-H_2 ($j_2 = 1 \rightarrow 1$) and ground state p-H_2 ($j_2 = 0 \rightarrow 0$) at 100, 300, and 500 K kinetic temperatures. Fig. 6 compares the rate coefficients of o-H_2 ($j_2 = 1 \rightarrow 1$) and excited p-H_2 ($j_2 = 2 \rightarrow 2$) for the same transitions and temperatures, while Fig. 7 shows the relation between state-to-state o-H_2 ($j_2 = 1 \rightarrow 1$) and thermalized p-H_2 rate coefficients. As can be seen in Fig. 5, the correlation between the collisional data calculated for collisions with

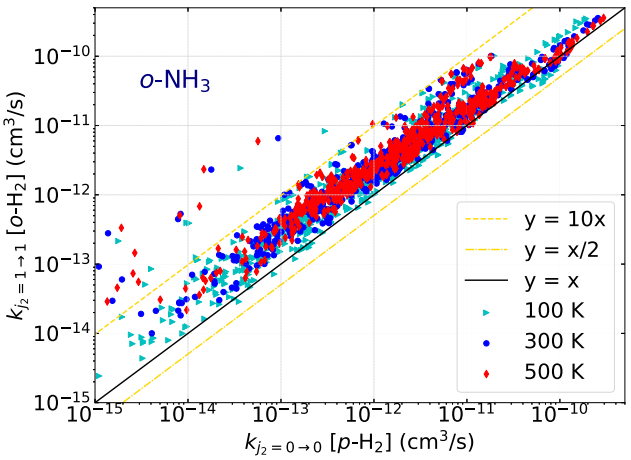

Figure 5. Ratio of the state-to-state rate coefficients for the collision of o-NH_3 with o-H_2 ($j_2 = 1 \rightarrow 1$) versus p-H_2 ($j_2 = 0 \rightarrow 0$). All rotational de-excitation transitions are considered below $\sim$800 $\rm cm^{-1}$ internal energy at kinetic temperatures of 100, 300, and 500 K.

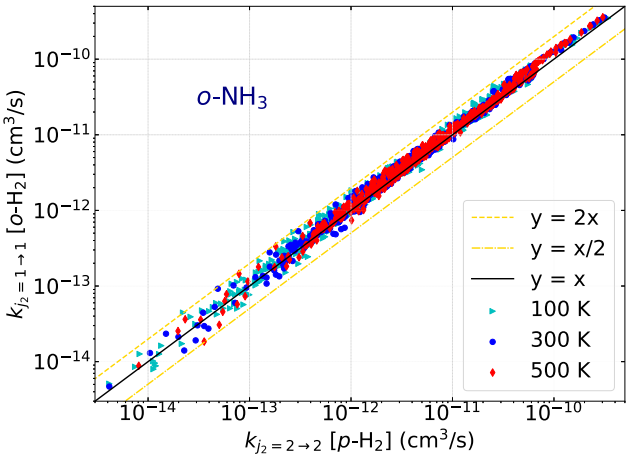

Figure 6. Same as Fig. 5 but the ratio is calculated from collisional data for o-H_2 ($j_2 = 1 \rightarrow 1$) and p-H_2 ($j_2 = 2 \rightarrow 2$) colliders.

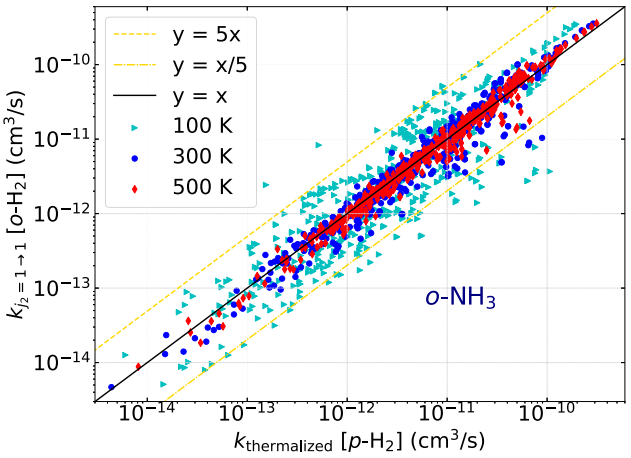

Figure 7. Same as Fig. 5 but the ratio is calculated from collisional data for o-H_2 ($j_2 = 1 \rightarrow 1$) and thermalized p-H_2 colliders.

o-H_2 and ground state p-H_2 is generally modest, as expected from the behaviour of the corresponding cross sections. For the majority of the transitions, we find that o-H_2 can de-excite ammonia more intensely, since the corresponding rate coefficients are significantly larger. Most commonly, we observe about 4–5 times larger $k(T)$ values in favour of this projectile, but for some low-magnitude transitions the differences can be larger than one order of magnitude, and even reach two orders of magnitude. Also, these largest deviations do not depend on the temperature. There is some correlation between the two data sets for the largest rate coefficients, greater than $\sim 10^{-10}$ cm^3 s^{-1}. In this range, the rate coefficients typically agree within 30–40 per cent, and the larger deviations are observed at 100 K. Our analysis again confirms that ground-state H_2 ($j_2 = 0$) cannot be used as a template for 'normal' H_2 in warm clouds, where its excited levels can be significantly populated.

Fig. 6 reveals different rate coefficient relationships. In this plot, the o-$H_2(j_2 = 1 \rightarrow 1)$ data are compared with excited p-$H_2(j_2 = 2 \rightarrow 2)$ and the correlation between them is much stronger: we observe differences up to a factor of 2 at most. The deviations are larger for less dominant transitions (below $\sim 10^{-12}$ cm^3 s^{-1}). For all others, the two sets of $k(T)$ are in a very good agreement, usually within 50 per cent. We found the following mean relative errors (involving all transitions in the statistics): 20.8, 17.0, and 15.9 per cent at 100, 300, and 500 K, respectively. It is worth noting that these differences may partially arise from the fact that $j_2 = 3$ was not included in the basis set for o-H_2 (the impact of adding $j_2 = 3$ can lead to a factor of $\sim$1.3 differences, see Fig. 1). The same tendencies were observed with the p-NH_3 rate coefficients. In general, all the effective rate coefficients in NH_3–H_2 collisions with $j_2 \geq 1$ are quantitatively similar at higher temperatures, independently from the nuclear spin symmetry of H_2, as was also found in the case of the NH_2D–H_2 (Daniel et al. 2014) and H_2O–H_2 (Daniel et al. 2011) collisions. Thus, in the absence of appropriate collisional data, H_2 in either $j_2 = 1$ or $j_2 = 2$ can be a reliable template for any excited states of o/p-$H_2(j_2 \geq 1)$.

In order to examine the direct impact of thermal averaging over H_2-population on the rate coefficient, we also analysed their relative ratio with respect to the state-to-state o-H_2 ($j_2 = 1$) data in Fig. 7. As can be seen in Fig. 7, we observe that at higher temperatures (500 K), the thermalized rate coefficients correlate with the state-to-state o-H_2 data. This correlation is not as strong as in the case of the p-$H_2(j_2 = 2 \rightarrow 2)$ data (see Fig. 6), but the general agreement at this temperature is usually within a factor of 2. While we found somewhat less coherence in this case, only some specific transitions possess larger ratios than a factor of 2 at 500 K, and these are exclusively the ones impacted by near-resonance effects. The absolute mean deviation is $\sim$15.4 per cent, which is very close to what was found in the case of the $j_2 = 2 \rightarrow 2$ versus $j_2 = 1 \rightarrow 1$ processes ($\sim$15.9 per cent). On the other hand, when analysing the ratios at 100 K, we found unexpectedly large deviations, usually within a factor of 5, but for some near-resonant transitions they can be as large as an order of magnitude. If we examine the magnitude of the H_2-inelastic transitions which contribute to the thermal average (see equation (2)), we can easily find the origin of these effects: in the case of transitions accompanied with a significant rotational energy transfer, *i.e.* when the internal energy change is larger than the energy gap between the $j_2 = 0$ and 2 p-H_2 levels, the $j_2 = 0 \rightarrow 2$ transition becomes very efficient, which significantly contributes to the thermalized rate coefficients at 100 K. Similar effects were reported also by Daniel et al. (2011). Since the considered NH_3 levels involve a large number of such transitions, we observe a strong change in the distribution of the relative ratios shown in Fig. 7 w.r.t. Fig. 6, and the corresponding thermalized rate coefficients over the p-H_2 states are significantly larger than those of for o-H_2 ($j_2 = 1 \rightarrow 1$). Such effects are probably also present in the case of collisions with o-H_2, but since the energy gap between the $j_2 = 1$, 3 levels is much higher ($\sim$587 cm^{-1}), the number of impacted transitions would be significantly less and are usually of low-magnitude (as expected from the energy-gap law). Thus, it is not advised to use thermalized p-H_2 rate coefficients to model the excitation due to o-H_2 at lower temperatures, but the differences between these collisional data is strongly decreasing at higher temperatures.

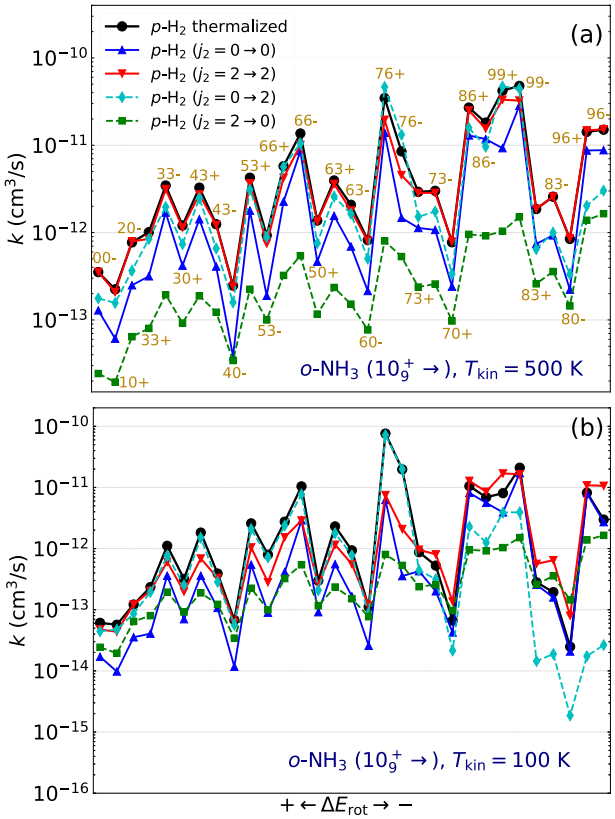

Figure 8. Propensity rules showing the variation of the rate coefficients for de-excitation transitions from the 10_9^+ state of o-NH_3 accompanied with different p-H_2-elastic/inelastic and thermally averaged processes at higher (500 K, panel a) and lower (100 K, panel b) kinetic temperatures. The transition energy (rotational energy difference, ΔE_{rot}) is decreasing from left to right (see Appendix A for the full description of rotational levels and energies).

3.3 Propensity rules

In Figs 8and9, the collisional propensity rules are analysed based on the state-to-state and thermalized rate coefficients. Fig. 8 presents $k(T)$ for all possible de-excitation paths from the 10_9^+ level of o-NH_3 at kinetic temperatures of 500 K (a) and 100 K (b). Both the ($j_2 = 0 \rightarrow 0$, $j_2 = 2 \rightarrow 2$) H_2-elastic as well as the ($j_2 = 0 \rightarrow 2$, $j_2 = 2 \rightarrow 0$) H_2-inelastic processes are analysed along with the thermally averaged p-H_2 rate coefficients. In Fig. 9, the collisional propensities for transitions out of the 9_7^- level of p-NH_3 are analysed, involving also de-excitation due to o-H_2 ($j_2 = 1 \rightarrow 1$) collision.

As one can see, there is no clear evidence for general propensity trends with respect to the quantum numbers, but the same qualitative behaviour is observed for all H_2-processes. In Fig. 8a, the transitions to states with $k = 0$ are usually the smallest. Also, there is a

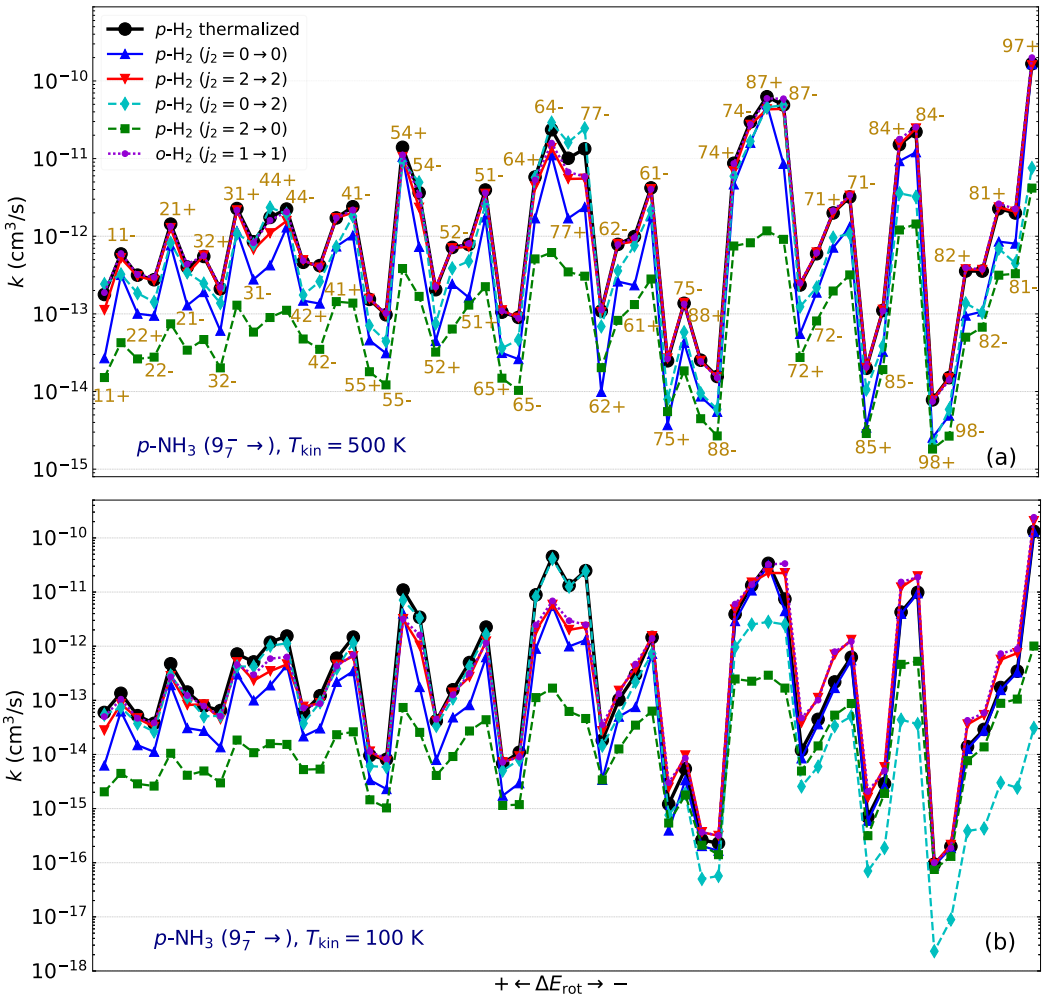

Figure 9. Same as Fig. 8 but for de-excitation transitions from the 9_7^- initial state of p-NH_3 at $T_{kin} = 500$ K (panel a) and $T_{kin} = 100$ K (panel b).

preference for transitions towards $j = k$ final states. Somewhat smaller differences are found for processes where only the inversion symmetry is changing (*e.g.* 6_3^+ and 6_3^-). We can observe some propensity tendencies for the transitions analysed, which are very similar both at 100 and 500 K, but there are no clear scaling rules that generally apply to all transitions. For example, in the case of p-NH_3 we found that the 9_7^+ and $8_7^\pm$ (*i.e.* $\Delta k = 0$) final states are the most dominant in Fig. 9, but there are some larger Δk transitions too with strong de-excitation rate coefficients, including the $8_4^\pm$ or $7_4^\pm$ channels. In general, the most favoured transitions are those when $\Delta k = 0$, 3 or even $\Delta k = 6$, while all other transitions are hindered and significantly less efficient, especially in the case of large-j jumps. This can be explained by the expansion terms of the PES. For example, in the case of $H_2(j_2 = 0)$ in the v_{lm} radial coefficients m has to be a multiple of 3 at arbitrary l. Transitions that change in the k-ladder are governed by terms with $m = \Delta k$, and these terms are smaller when m increases. This makes favourable those transitions, when Δk is a multiple of 3 (*e.g.* $9_7^- \rightarrow 8_7^\pm$, $8_4^\pm$, $8_1^\pm$). For transitions when Δk is not a multiple of 3, higher order expansion terms are required, since these states are not directly coupled (Rist et al. 1993; Loreau & van der Avoird 2015). These effects are also similar to the dipole selection rules, which favour $\Delta j = 0{,}1$ and $\Delta k = 0$ transitions. No clear propensities can be observed w.r.t. the symmetry index or inversion symmetry: transitions to a given j_k level with $\pm$ are comparable and imply rather similar rate coefficients. However, it is worth mentioning that we found pronounced tendencies involving inversion symmetry change in the most efficient $\Delta j = 1$; $\Delta k = 0$ transitions (*e.g.* see the $10_9^+ \rightarrow 9_9^-$ and the $9_7^- \rightarrow 8_7^+$ processes in Figs. 8–9). These can be also explained due to the expansion terms of the PES. The symmetry-changing transitions require that $l + m$ to be odd, while the transitions that conserve inversion require terms with even $l + m$ (Rist et al. 1993). These rules are more general for $H_2(j_2 = 0)$, since for $H_2(j_2 \geq 1)$ additional coupling terms are involved in the expansion scheme. We also found that, in general, the propensities are rather invariant to temperature. Stronger propensities are observed usually with respect to the projection quantum number k as opposed to the change in the main rotational quantum number j, so that the collision aims to conserve the projection of the NH_3 angular momentum on the C_3 molecular axis.

Both in the case of o-NH_3 (Fig. 8) and p-NH_3 (Fig. 9) de-excitation transitions, only the H_2-elastic processes are dominant when the rotational energy release (ΔE_{rot}) is low, and their statistical average dominates in the thermalized rate coefficients. With increasing ΔE_{rot}, the $j_2 = 0 \rightarrow 2$ H_2-inelastic process becomes more significant due to the more efficient rotational energy transfer. We can clearly locate those transitions (with $\Delta E_{rot} \simeq 336$–$369\,cm^{-1}$), in which the near-resonant effects are the strongest. For these, the thermalized rate coefficients can be about an order of magnitude larger than any of

the pure H_2-elastic data. At 100 K, the dependence of the magnitude of H_2-inelastic transitions on ΔE_{rot} is more pronounced: when the energy release is small, the $j_2 = 0 \rightarrow 2$ process is very weak, and the thermalized rate coefficients are almost entirely determined by the $j_2 = 0 \rightarrow 0$ rate coefficients. At higher ΔE_{rot}, however, the $j_2 = 0 \rightarrow 2$ channel is significantly stronger, and its contribution becomes dominant in the thermally averaged collisional data.

4 CONCLUSIONS

In this paper, we have presented rotational (de)excitation cross sections and rate coefficients for the collision of ammonia (NH_3) with molecular hydrogen (H_2). Both the *ortho/para* nuclear spin configurations were considered in the case of the colliding partners, so that all four possible nuclear symmetry combinations of the NH_3–H_2 complex are studied. In the case of *para*-H_2, the thermally averaged rate coefficients were also computed based on the temperature-dependent relative population of $j_2 = 0$ and 2 hydrogen levels.

The cross sections possess pronounced resonance properties, typically up to collision energies of 250–300 cm^{-1}, which correlate well with the depth of the interaction potential. The resonance behaviour is less pronounced in the case of collisions with excited $H_2(j_2 > 0)$ due to the strong overlap between the dense peaks. At higher collision energies, the cross sections show the usual, monotonic decreasing behaviour. We found very significant differences (typically within a factor of 2–5) between the collisional data calculated with *ortho*-$H_2(j_2 = 1)$ and ground state *para*-$H_2(j_2 = 0)$ colliders, in favour of the former. However, there is a good overall agreement between the state-to-state cross sections and rate coefficients obtained for H_2-elastic collisions with *ortho*-$H_2(j_2 = 1)$ and excited *para*-$H_2(j_2 = 2)$, which are related to the l_2 expansion terms of the PES. We have presented a comparison at the level of cross sections with the most accurate data for collisions of NH_3 with helium (Yang & Stancil 2008) and hydrogen atoms (Bouhafs et al. 2017). We found large relative differences (typically 1–2 orders of magnitude) with respect to our H_2 collisional data, but we did not observe any systematic scaling rules between the different projectiles. The mutual analysis of thermally averaged and state-to-state rate coefficients has also showed that the impact due to the $j_2 = 0 \rightarrow 2$ excitation of *para*-H_2 can be very significant. The thermalized rate coefficients thus can have a much larger magnitude compared to the respective state-to-state data, especially when a near-resonance occurs between *para*-H_2 and NH_3 transitions. We can draw a conclusion that neither He and H, nor the simple ground state *p*-$H_2(j_2 = 0)$ can be used as a template for appropriate modelling of collisions with molecular hydrogen at high temperatures ($\gtrsim$100 K). Clearly, projectile- and state-specific, accurate collisional data are needed to interpret the ammonia observations in warm interstellar environments, considering at least the three lowest rotational levels of $H_2(j_2 = 0, 1, 2)$.

When analysing the collisional propensity rules, we did not find any universal tendencies for the favourable de-excitation routes that can be validated for arbitrary rotational states. Nevertheless, one can observe some general trends, which are usually related to the connections between the quantum numbers of the initial and final rotational states. These generally correspond to the well known dipole selection rules. For example, some propensities are found for a well-defined combination of j and k rotational quantum numbers, which clearly depend on the parameters of the initial state. Among them, the $\Delta j = 0, \pm 1$ transitions are the most favourable, but only when $\Delta k = 0$. For transitions involving different k-ladders, we found that $\Delta k = -3$ or -6 are very efficient de-excitation routes too, but positive jumps in the k-ladder are not favourable (obviously, the opposite rule holds for the reverse excitation transitions). In general, we observed about an order of magnitude lower rate coefficients towards final states obeying $|\Delta k| = 1, 2$ with respect to the initial state. Consequently, the collisional propensity rules are more stringent and more pronounced in relation to the projection quantum number k than in the case of the main rotational quantum number j. Our new set of state-to-state and thermalized rate coefficients should help to accurately model non-LTE rotational spectra of NH_3 (within $\nu_2 = 0$) up to about 500 K, *i.e.* covering warm interstellar and circumstellar environments.

ACKNOWLEDGEMENTS

We acknowledge financial support from the European Research Council (Consolidator Grant COLLEXISM, Grant Agreement No. 811363) and the Programme National 'Physique et Chimie du Milieu Interstellaire' (PCMI) of CNRS/INSU with INC/INP cofunded by CEA and CNES. We wish to acknowledge the support from the CEA/GENCI for awarding us access to the TGCC/IRENE supercomputer within the A0110413001 project. F.L. acknowledges the Institut Universitaire de France.

DATA AVAILABILITY

The data that support the findings of this study are available within the article and its supplementary material at MNRAS online. The collisional data presented in this article will be made publicly available also through the EMAA https://emaa.osug.fr/ (EMAA 2021), LAMDA https://home.strw.leidenuniv.nl/~moldata/ (van der Tak et al. 2020) and BASECOL https://basecol.vamdc.eu/ (Dubernet et al. 2012) data bases.

REFERENCES

Alexander M., Dagdigian P., Werner H.-J., Kłos J., Desrousseaux B., Raffy G., Lique F., 2023, Comput. Phys. Commun., 289, 108761
Bőgner R., Csengeri T., Montillaud J., Wienen M., Schneider N., Wyrowski F., Motte F., Tóth L. V., 2022, A&A, 667, A137
Bouhafs N., Rist C., Daniel F., Dumouchel F., Lique F., Wiesenfeld L., Faure A., 2017, MNRAS, 470, 2204
Candelaria T. M., Mills E. A. C., Meier D. S., Ott J., Mangum J. G., K. Mangum, et al., 2016. Widespread Hot Ammonia in the Central Kiloparsec of the Milky Way. In *American Astronomical Society Meeting Abstracts #227*, 227, 341
Cheung A. C., Rank D. M., Townes C. H., Thornton D. D., Welch W. J., 1968, Phys. Rev. Lett., 21, 1701
Daly P. W., Oka T., 1970, The J. Chem. Phys., 53, 3272
Danby G., Flower D. R., Valiron P., Schilke P., Walmsley C. M., 1988, MNRAS, 235, 229
Daniel F. et al., 2016, MNRAS, 457, 1535
Daniel F., Dubernet M.-L., Grosjean A., 2011, A&A, 536, A76
Daniel F., Faure A., Wiesenfeld L., Roueff E., Lis D. C., Hily-Blant P., 2014, MNRAS, 444, 2544
De Simone M. et al., 2022, ApJL, 935, L14
Dubernet M. L., et al., 2012, "BASECOL2012: A collisional database repository and web service within Virtual Atomic and Molecular Data Center (VAMDC)". A&A, 553, 50
EMAA, 2021, EMAA. UGA, CNRS, CNRS-INSU, OSUG. Available from: https://dx.doi.org/10.17178/EMAA
Faure A., Valiron P., Wernli M., Wiesenfeld L., Rist C., Noga J., Tennyson J., 2005, J. Chem. Phys., 122, 221102
Feng S., Liu H. B., Caselli P., Burkhardt A., Du F., Bachiller R., Codella C., Ceccarelli C., 2022, ApJL, 933, L35
Galloway-Sprietsma M., Shirley Y. L., Di Francesco J., Keown J., Scibelli S., Sipilä O., Smullen R., 2022, MNRAS, 515, 5219

Gao Z., Loreau J., van der Avoird A., van de Meerakker S. Y. T., 2019, Phys. Chem. Chem. Phys., 21, 14033
Green S., 1980, J. Chem. Phys., 73, 2740
Ho P. T. P., Townes C. H., 1983, ARA&A, 21, 239
Lanza M., Kalugina Y., Wiesenfeld L., Lique F., 2014, J. Chem. Phys., 140, 064316
Loreau J., van der Avoird A., 2015, J. Chem. Phys., 143, 184303
Ma Q., van der Avoird A., Loreau J., Alexander M. H., van de Meerakker S. Y. T., Dagdigian P. J., 2015, J. Chem. Phys., 143, 044312
Machin L., Roueff E., 2005, J. Phys. B: At. Mol. Opt. Phys., 38, 1519
Maret S., Faure A., Scifoni E., Wiesenfeld L., 2009, MNRAS, 399, 425
Mills E. A. C., Corby J., Clements A. R., Butterfield N., Jones P. A., Cunningham M. R., Ott J., 2018, ApJ, 869, 121
Mills E. A. C., Morris M. R., 2013, ApJ, 772, 105
Oka T., 1968, J. Chem. Phys., 48, 4919
Pickett H. M., Cohen E. A., Drouin B. J., 2010, J. Quant. Spectrosc. Radiat. Transf., 111, 1617
Rajamäki T., Miani A., Halonen L., 2003, J. Chem. Phys., 118, 10929
Rist C., Alexander M. H., Valiron P., 1993, J. Chem. Phys., 98, 4662
Rist C., Faure A., 2012, J. Math. Chem., 50, 588
Roueff E., Lique F., 2013, Chem. Rev., 113, 8906
Schleipen J., ter Meulen J., Offer A., 1993, Chem. Phys., 171, 347
Sipilä O., Caselli P., Redaelli E., Juvela M., Bizzocchi L., 2019, MNRAS, 487, 1269
Tkác O., Saha A. K., Loreau J., Ma Q., Dagdigian P. J., Parker D. H., van der Avoird A., Orr-Ewing A. J., 2015, Mol. Phys., 113, 3925
van der Tak F. F. S., Lique F.,Faure A.,Black J. H,van Dishoeck E. F.,2020, Atoms, 8, 15
Willey D. R., Timlin R. E., Jr, Merlin J. M., Sowa M. M., Wesolek D. M., 2002, ApJS, 139, 191
Wong K. T., Menten K. M., Kamiński T., Wyrowski F., Lacy J. H., Greathouse T. K., 2018, A&A, 612, A48
Yang B. H., Stancil P. C., 2008, Eur. Phys. J. D, 47, 351
Zhou D. D., Wu G., Esimbek J., Henkel C., Zhou J. J., Li D. L., Ji W. G., Zheng X. W., 2020, A&A, 640, A114

SUPPORTING INFORMATION

Supplementary data are available at *MNRAS* online.
Please note: Oxford University Press is not responsible for the content or functionality of any supporting materials supplied by the authors. Any queries (other than missing material) should be directed to the corresponding author for the article.

APPENDIX A: ROTATIONAL LEVELS OF AMMONIA FOR WHICH COLLISIONAL DATA ARE CALCULATED IN THIS WORK

Table A1. The full list of rotational energy levels for *ortho*-NH_3 considered in the present study. The corresponding energies are taken from JPL data base (Pickett, Cohen & Drouin (2010), Species Tag: 17002, version 5, compiled by S. Yu, 1 Sep. 2010). The rotational energies computed by the HIBRIDON code, which were used in the scattering calculations, are in a good overall agreement with these data, with a mean deviation of ∼1 per cent.

ortho-NH_3 rotational levels					
State label	Internal energy [cm^{-1}]	Rotational state $j_k^{\pm}$	State label	Internal energy [cm^{-1}]	Rotational state $j_k^{\pm}$
(1)	0.000000	0_0^-	(18)	421.664932	7_6^+
(2)	19.096483	1_0^+	(19)	422.429625	7_6^-
(3)	59.619617	2_0^-	(20)	520.828585	7_3^+
(4)	85.068186	3_3^+	(21)	521.429579	7_3^-
(5)	85.864408	3_3^-	(22)	553.599742	7_0^+
(6)	118.444459	3_0^+	(23)	579.986473	8_6^+
(7)	164.537707	4_3^+	(24)	580.677592	8_6^-
(8)	165.294507	4_3^-	(25)	591.793694	9_9^+
(9)	198.500538	4_0^-	(26)	592.710260	9_9^-
(10)	263.723260	5_3^+	(27)	678.494549	8_3^+
(11)	264.433261	5_3^-	(28)	679.043432	8_3^-
(12)	282.781115	6_6^+	(29)	711.559858	8_0^-
(13)	283.616894	6_6^-	(30)	757.592095	9_6^+
(14)	296.848422	5_0^+	(31)	758.209168	9_6^-
(15)	382.525089	6_3^+	(32)	789.887816	10_9^+
(16)	383.184131	6_3^-	(33)	790.695217	10_9^-
(17)	416.094413	6_0^-	–	–	–

The complete set of the rotational levels considered in this work for both *ortho*/*para*-NH_3 target species are given in Tables A1 and A2, respectively. It is worth to emphasize that for the definition of the NH_3 levels, the notation with the inversion symmetry +/− is used rather than the ϵ symmetry index.

Table A2. The same as Table A1, but for *para*-NH_3 rotational levels considered in the present study.

para-NH_3 rotational levels								
State label	Internal energy [cm^{-1}]	Rotational state $j_k^{\pm}$	State label	Internal energy [cm^{-1}]	Rotational state $j_k^{\pm}$	State label	Internal energy [cm^{-1}]	Rotational state $j_k^{\pm}$
(1)	15.379581	1_1^+	(22)	282.823311	5_2^-	(43)	539.051568	7_2^+
(2)	16.169945	1_1^-	(23)	293.174912	5_1^+	(44)	539.628351	7_2^-
(3)	44.002570	2_2^+	(24)	293.836648	5_1^-	(45)	549.965265	7_1^+
(4)	44.793872	2_2^-	(25)	323.575629	6_5^+	(46)	550.527020	7_1^-
(5)	55.145322	2_1^+	(26)	324.333901	6_5^-	(47)	620.272295	8_5^+
(6)	55.915816	2_1^-	(27)	356.790867	6_4^+	(48)	620.899680	8_5^-
(7)	103.628679	3_2^+	(28)	357.491173	6_4^-	(49)	653.077294	8_4^+
(8)	104.390346	3_2^-	(29)	373.455885	7_7^+	(50)	653.656966	8_4^-
(9)	114.743221	3_1^+	(30)	374.313652	7_7^-	(51)	654.853426	9_8^+
(10)	115.484885	3_1^-	(31)	400.854489	6_2^+	(52)	655.642555	9_8^-
(11)	138.564636	4_4^+	(32)	401.484415	6_2^-	(53)	696.601988	8_2^+
(12)	139.369840	4_4^-	(33)	411.830973	6_1^+	(54)	697.123674	8_2^-
(13)	183.035703	4_2^+	(34)	412.444450	6_1^-	(55)	707.445146	8_1^+
(14)	183.759649	4_2^-	(35)	462.219782	7_5^+	(56)	707.953272	8_1^-
(15)	194.112947	4_1^+	(36)	462.913756	7_5^-	(57)	710.063268	9_7^+
(16)	194.817912	4_1^-	(37)	476.471115	8_8^+	(58)	710.754928	9_7^-
(17)	204.475777	5_5^+	(38)	477.355693	8_8^-	(59)	719.386458	10_{10}^+
(18)	205.294109	5_5^-	(39)	495.241772	7_4^+	(60)	720.340610	10_{10}^-
(19)	237.859254	5_4^+	(40)	495.882832	7_4^-	(61)	797.581238	9_5^+
(20)	238.614878	5_4^-	(41)	532.100983	8_7^+	(62)	798.141563	9_5^-
(21)	282.143792	5_2^+	(42)	532.875927	8_7^-	–	–	–

This paper has been typeset from a TEX/LATEX file prepared by the author.